Journal of Sound and Vibration (1997) **205**(1), 57–80

FEEDBACK STRUCTURE-BORNE SOUND CONTROL OF A FLEXIBLE PLATE WITH AN ELECTROMAGNETIC ACTUATOR: THE PHASE LAG PROBLEM

M. Z. Ren

Vibration Control Laboratory, *Kyowa Metal Works Co*., *Ltd*, *Fukuura* 1-1-1, *Kanazawa-ku*, *Yokohama* 236, *Japan*

AND

K. Seto

Department of Mechanical Engineering, *Nihon University*, 1-8 *Kanda Surugadai*, *Chiyodo-ku*, *Tokyo* 101, *Japan*

AND

F. Doi

Vibration Control Laboratory, *Kyowa Metal Works Co*., *Ltd*, *Fukuura* 1-1-1, *Kanazawa-ku*, *Yokohama* 236, *Japan*

(*Received* 28 *May* 1996, *and in final form on* 11 *February* 1997)

In this paper an experimental study is presented on active control of a clamped plate at audio frequencies by using feedback controller and electromagnetic actuator. The controller is designed with modern control theory on a lumped parameter model of the plate, and is then implemented in experiments to control the real structure. In practice, the optimal control force cannot be generated exactly as desired due to the non-ideal characteristics of the control system. Several factors such as A/D and D/A convertors, velocity estimation through approximate differentiation, and the electromagnetic actuator are examined in respect to their frequency features. An analytical model is developed to predict the phase lag of the actual control force to the designed control force. It is shown that if the phase lag is over 90 degrees, the control system will become unstable. Two techniques are discussed for improving the system performance that is mainly affected by the electromagnetic actuator when the high speed sampling and processing device is used as the controller. The simple and practical method is to employ a phase-lead compensation network in the control circuit. Another one that is more fundamental is to incorporate the characteristics of the actuator into the system by feeding back the current passing through the actuator into the controller. Various experiments are carried out to verify the analysis and the proposed methods, and the potentials of the electromagnetic actuator in controlling the high frequency vibration and noise are therefore demonstrated.

1. INTRODUCTION

In recent years, active structure control has come to real application in some fields such as civil engineering, where the active means of protective design of tall structures such as buildings and bridge towers against adverse environmental loads have prevailed [1]. However, the research of active vibration control for the purpose of reducing mechanical noise has not yet seen so many successful applications. The main obstacle perhaps is that

0022–460X/97/310057 + 24 $25.00/0/sv970999

the mechanical noise and vibration are often in a fairly high frequency range, which may present some difficulties in view of the capacity of the current control hardware and software. Nevertheless, the research and development of this active vibration control technique, also known as active structural acoustic control (ASAC) [2], has been experiencing concrete progress owing to the rapid development of microprocessors and control algorithms.

The feedforward approach based on the adaptive signal processing technique has been the dominating method in the community of active noise and structural acoustic control [3, 4]. On the other hand, it is only recently that the feedback approach based on modern control theory, which is well developed for the control of dynamic systems, has comparatively received more attention in active noise and structural acoustics control [5–8]. As pointed out by Fuller *et al*. [2], there has been a great deal of theoretical work concerning the feedback control of finite structures, with experimental investigations being rather thin on the ground. This is particularly true in the case of controlling structure vibration in the audio frequency range. This paper, an experimental study is presented on feedback control of a flexible plate at audio frequencies with an electromagnetic actuator. The controller is designed in state space by using the linear quadratic optimal control theory (LQ theory) on the basis of a lumped parameter model of the plate, and then is implemented in experiments to control the real structure. The modelling and the control design are, however, not the concern of the present paper; the purpose of this paper is to investigate the practical problem involved in the actual control system, namely, the phase lag problem. This is a very important problem in feedback control systems, especially on occasions when an electromagnetic actuator is used to control high frequency vibration and noise. Perhaps everyone working in feedback control may consciously or unconsciously meet this problem but, it seems, to the authors' knowledge, that few have been reported in the literature to have dealt with it in special detail. Fuller *et al*. [2] examined, in a general way, the effects of the delays in the feedback loop on the system dynamics, such as the influence on the effective mass, effective stiffness and effective damping etc. In reference [9] the role of the control–structure interaction, showing the importance of accounting for the actuator (hydraulic type) dynamics in modelling the system, was studied.

In general, the phase lag depends on the hardware (sensor, actuator, processor, etc.) and the software (control method and algorithm). In this paper, the control object under study is a clamped thin rectangular steel plate. The control system constitution is typical in numerical control; that is, the analog vibration signals detected by the sensors are fed into the controller (computer) through A/D convertors, and the calculated digital control signal is supplied to the actuator through D/A convertors. As has been stated, an electromagnetic actuator, which is an important type of actuator in the active vibration and noise control field, is employed in this research. The vibration displacements are measured directly, while the velocities are estimated through the finite difference algorithm. In this investigation, the features of the various elements involved in the control loop are examined in respect to the frequency characteristics. Consequentially, a simple analytical model is developed to predict the phase difference between the ideal control force and the actual force of the system. It is observed that the absolute value of this difference should not exceed 90 degrees; otherwise, it will lead to positive feedback and deteriorate control robustness. The use of a high speed signal processor (DSP) can essentially alleviate the phase lag problems related to the sampling rate, but it does not help much when the electromagnetic actuator dominates the time delay of the whole loop. It is demonstrated that phase compensation is a useful way to offset the effects of the actuator. A more fundamental way is to model the actuator dynamics into the augmented system via the current feedback method.

Finally, various experiments are carried out to verify the analysis and the methods presented in this paper.

2. OUTLINE OF CONTROL SCHEME

The steel plate under study in this paper is a rectangular plate with a size of $600 \times 400 \times 1{\cdot}2$ mm. All the edges are clamped by frames and the plate is covered on to a box for the convenience of studying the noise transmission problem (therefore the plate is backed by an air cavity). This is a continuous system with distributed parameters (infinite degrees of freedom). In order to present the system in state equation in a finite number of state variables, it is necessary to set up a reduced order model for the system. Seto and Mitsuta [10] have developed a modelling method to create a lumped parameter model for distributed system, and a controller will be designed on the basis of this lumped system. Following this method, a lumped parameter system with nine degrees-of-freedom

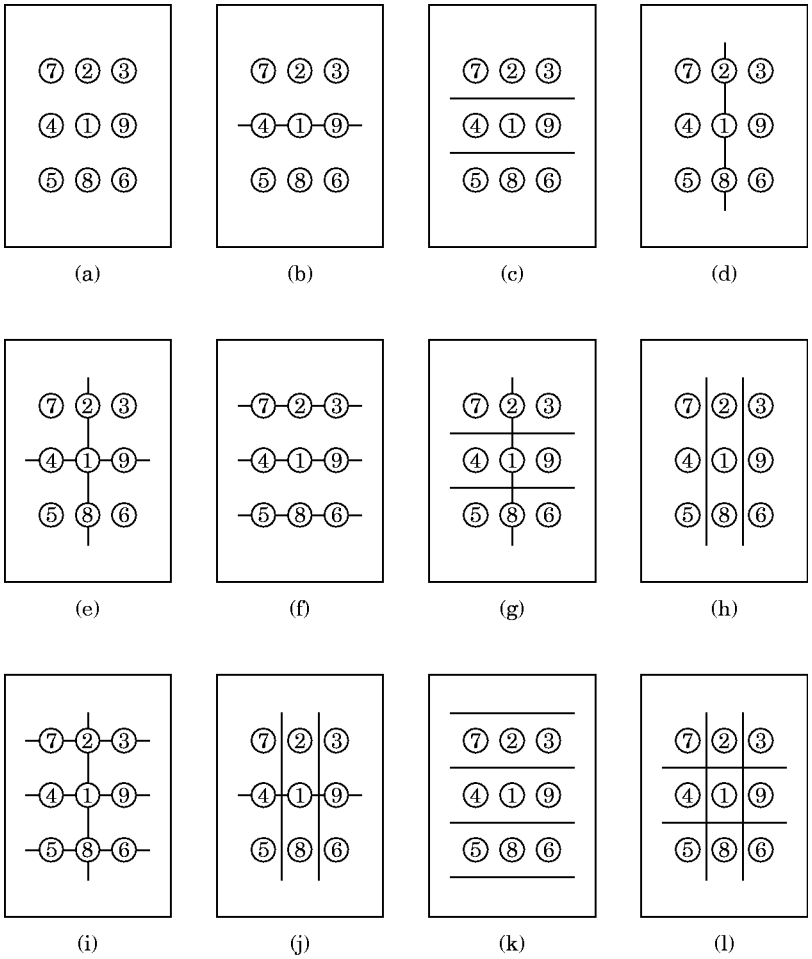

Figure 1. The first twelve mode shapes of the plate depicted by nodal lines. The circles and numbers refer to the positions of the modelling mass points. (a) First mode (1, 1), 44 Hz; (b) second mode (1, 2), 63 Hz; (c) third mode (1, 3), 98 Hz; (d) fourth mode (2, 1), 102 Hz; (e) fifth mode (2, 2), 125 Hz; (f) sixth mode (1, 4), 154 Hz; (g) seventh mode (2, 3), 158 Hz; (h) eighth mode (3, 1), 189 Hz; (i) ninth mode (2, 4), 215 Hz; (j) tenth mode (3, 2), 220 Hz; (k) eleventh mode (1, 5), 228 Hz; (l) twelfth mode (3, 3), 253 Hz.

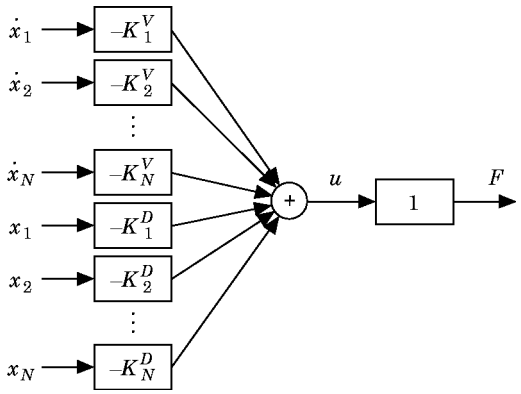

Figure 2. A diagram of the ideal control system.

(DOF) has been established to represent the nine of the first 12 vibration modes of the plate [11]. The modelling procedure is not the concern of the present paper, and readers are referred to reference [11] for details. Here for illustration, the first 12 mode shapes of the plate obtained by experimental modal analysis are explicitly depicted in Figure 1, using nodal lines. Also shown in this figure are the locations of the lumped modelling mass points (small circles). With the allocation of the mass points as given in Figure 1, this lumped parameter model does not account for the sixth and ninth modes of the plate, since all of the mass points are located at the modal nodes. It also does not incorporate the 11th mode and the modes higher than the 12th mode. Therefore, the modes under investigation are the first, second, third, fourth, fifth, seventh, eighth, tenth and the twelfth. It has been verified that the model can represent the dynamics of these nine modes of the plate very well at the modelling points. The standard LQ control theory can be conveniently formulated on this lumped model by using the state space approach.

Suppose that one actuator is installed at the mass point 1 in controlling this lumped system. The system can then be described by the following motion equations:

$$m_1\ddot{x}_1 + c\dot{x}_1 + \left(k_1 + \sum_{j=1}^{9} k_{1j}\right)x_1 - \sum_{j=2}^{9} k_{1j}x_j = f_a, \tag{1a}$$

$$m_i\ddot{x}_i + \left(k_i + \sum_{\substack{j=1\\ j\neq i}}^{9} k_{ij}\right)x_i - \sum_{\substack{j=1\\ j\neq i}}^{9} k_{ij}x_j = 0, \qquad i = 2, \ldots, 9. \tag{1b}$$

Here, x_i refers to the displacement of mass i, m_i is the ith mass, k_i is the stiffness of the spring connecting the ith mass and the ground, and k_{ij} refers to the spring between the ith mass and the jth mass. These mass and stiffness parameters are determined in the modelling procedure. Since in the present study the clamped plate is backed by an air cavity

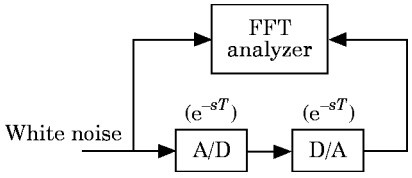

Figure 3. The arrangement for measuring the transfer function of the A/D and D/A convertors.

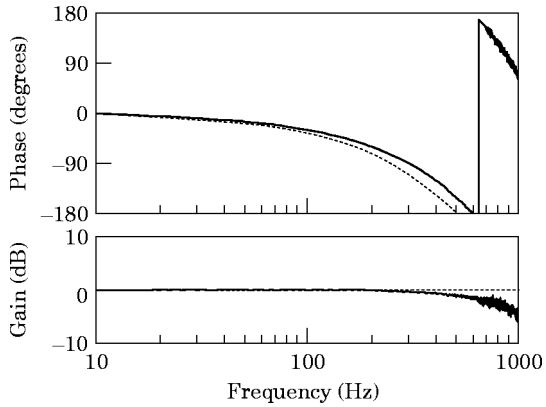

Figure 4. Bode plots of the A/D and D/A convertors. ———, Measured; ------, the term e^{-2sT}.

that is found to have a strong damping effect on the first mode of the plate, the effect has been roughly taken into account by the measured damping coefficient c in equation (1a). f_a is the control force generated by the actuator; if an ideal electromagnetic actuator is assumed, it can be expressed as

$$f_a = K_v u, \tag{2}$$

where K_v refers to the voltage-force coefficient of the electromagnetic actuator, and u is the control signal (voltage) supplied to the actuator.

Introducing a state vector

$$\mathbf{X} = [\dot{x}_1 \quad \dot{x}_2 \quad \cdots \quad \dot{x}_9 \quad x_1 \quad x_2 \quad \cdots \quad x_9]^{\mathrm{T}}, \tag{3}$$

the system can be presented in state space;

$$\dot{\mathbf{X}} = \mathbf{A}\mathbf{X} + \mathbf{b}u. \tag{4}$$

The state matrix $\mathbf{A}$ is given as

$$\mathbf{A} = \begin{bmatrix} -\mathbf{M}^{-1}\mathbf{C} & -\mathbf{M}^{-1}\mathbf{K} \\ \mathbf{I} & \mathbf{0} \end{bmatrix}_{18 \times 18}, \tag{5}$$

where $\mathbf{M}$ and $\mathbf{K}$ are the mass matrix and the stiffness matrix of the discrete system respectively, $\mathbf{I}$ is a (9×9) unit matrix, $\mathbf{0}$ is a (9×9) null matrix, and $\mathbf{C}$ is the damping matrix:

$$\mathbf{C} = \mathrm{diag}\,[c \quad 0 \quad 0 \quad 0 \quad 0 \quad 0 \quad 0 \quad 0 \quad 0]. \tag{6}$$

The state matrix $\mathbf{b}$ takes the form

$$\mathbf{b} = K_v[1/m_1 \quad 0 \quad 0 \quad 0 \quad 0 \quad 0 \quad 0 \quad 0 \quad 0 \quad 0 \quad 0 \quad 0 \quad 0 \quad 0 \quad 0 \quad 0 \quad 0 \quad 0 \quad 0 \quad]^{\mathrm{T}}. \tag{7}$$

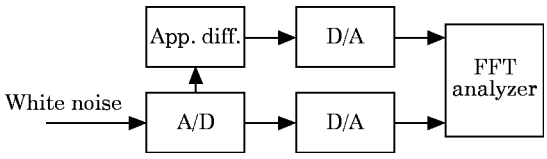

Figure 5. The arrangement for measuring the transfer function of the approximation differential element.

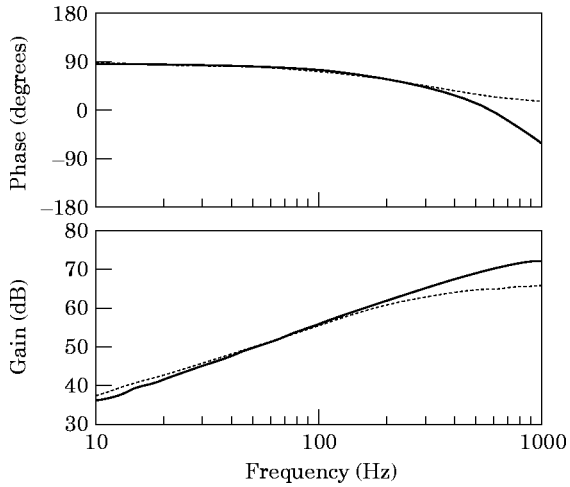

Figure 6. Bode plots of the approximation differential element. ———, Measured; -----, theory.

On the basis of LQ control theory, this system can be optimally controlled by the control value u that minimizes the following quadratic performance index:

$$J = \int_0^\infty (\mathbf{X}^T\mathbf{Q}\mathbf{X} + u^2 r)\, \mathrm{d}t, \tag{8}$$

where $\mathbf{Q}$ is the state weighting matrix and r is the control weighting factor. In this paper $\mathbf{Q}$ is a diagonal matrix with the components weighting the velocity states being assigned value one and the rest zero. The corresponding control value is obtained as

$$u = -r^{-1}\mathbf{b}^T\mathbf{P}\mathbf{X} = -\mathbf{K}_0\mathbf{X}, \tag{9}$$

where $\mathbf{K}_0$ is the feedback gain and $\mathbf{P}$ is the solution of the Riccati equation

$$\mathbf{P}\mathbf{A} + \mathbf{A}^T\mathbf{P} - \mathbf{P}\mathbf{b}r^{-1}\mathbf{b}^T\mathbf{P} + \mathbf{Q} = 0, \tag{10}$$

which can be solved by using the software Matlab (The Math Works Inc.).

The above control scheme needs to monitor the states (displacement and velocity) at nine mass points. In order to reduce the number of sensors required, the sub-optimal control theory [12] is adopted here so that only the state variables at three mass points (point 1, point 2 and point 8 in Figure 1) are to be measured for the feedback control. Assume $\mathbf{Z}$ to be a substate vector, the elements of which consist of the measured state variables at the three points, then the following transformation stands:

$$\mathbf{Z} = \mathbf{S}\mathbf{X}, \tag{11}$$

$$\mathbf{S} = \begin{bmatrix} 1 & 0 & 0 & 0 & 0 & 0 & 0 & 0 & 0 & 0 & 0 & 0 & 0 & 0 & 0 & 0 & 0 & 0 \\ 0 & 1 & 0 & 0 & 0 & 0 & 0 & 0 & 0 & 0 & 0 & 0 & 0 & 0 & 0 & 0 & 0 & 0 \\ 0 & 0 & 0 & 0 & 0 & 0 & 0 & 1 & 0 & 0 & 0 & 0 & 0 & 0 & 0 & 0 & 0 & 0 \\ 0 & 0 & 0 & 0 & 0 & 0 & 0 & 0 & 0 & 1 & 0 & 0 & 0 & 0 & 0 & 0 & 0 & 0 \\ 0 & 0 & 0 & 0 & 0 & 0 & 0 & 0 & 0 & 0 & 1 & 0 & 0 & 0 & 0 & 0 & 0 & 0 \\ 0 & 0 & 0 & 0 & 0 & 0 & 0 & 0 & 0 & 0 & 0 & 0 & 0 & 0 & 0 & 0 & 1 & 0 \end{bmatrix}. \tag{12}$$

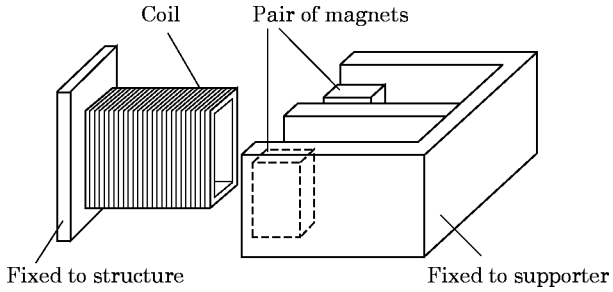

Figure 7. The structure of the electromagnetic actuator.

Accordingly, the control value can be expressed as

$$u = -\mathbf{K}_s \mathbf{Z}, \tag{13}$$

where the sub-optimal feedback gain $\mathbf{K}_s$ can be determined by the minimum norm method [12] as follows

$$\mathbf{K}_s = \mathbf{K}_0 \mathbf{S}^{\mathrm{T}} (\mathbf{S}\mathbf{S}^{\mathrm{T}})^{-1} \mathbf{S}. \tag{14}$$

In the preceding discussion it has been assumed that only one actuator is installed at mass point 1 (the plate centre). This fixing point is also located on the nodal lines of the second, fourth, fifth, seventh, ninth and tenth modes of the plate, and therefore, these modes are uncontrollable. The controllable modes are the first, third, eighth and twelfth modes, which are found to have relatively high sound radiation efficiencies.

3. PHASE LAGS OF CONTROL SYSTEM

3.1. IDEAL CONTROL FORCE

In the above section it has been illustrated that on the basis of the dynamics of the reduced order model, a set of optimal feedback gain can be calculated. For the case in which all of the state variables are supposed to be correctly measured and the actuating device has ideal characteristics, the optimal control force can then be generated as

$$F = -\left(\sum_{n=1}^{N} K_n^V \dot{x}_n + \sum_{n=1}^{N} K_n^D x_n \right), \tag{15}$$

where K_n^V and K_n^D are the optimal feedback gain for the velocity terms and the displacement terms respectively. This is the ideal situation as depicted in Figure 2. The control force in this situation is referred to as the ideal force or the designed force.

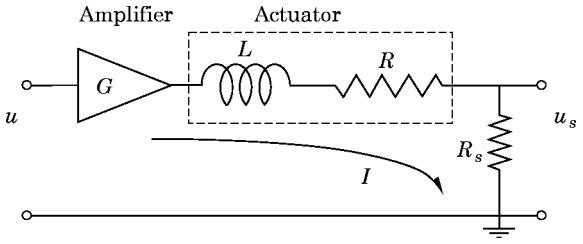

Figure 8. The equivalent circuit of the actuator and the related amplifier.

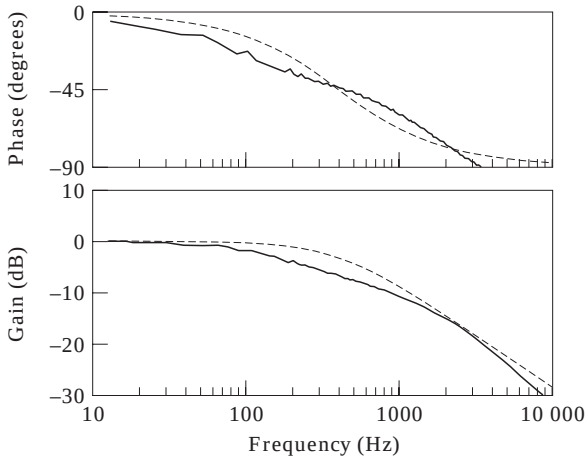

Figure 9. Bode plots of the amplifier and actuator. ———, Measured; ------, the term $1/(1+\tau s)$ with $\tau = 2.5$ ms.

3.2. EXAMINATION OF SYSTEM CHARACTERISTICS

However, for practical system there are some deviations from the ideal conditions. A preliminary investigation has shown that for the control system of the present concern, there are several factors the non-ideal frequency characteristics of which have an influence on the control performance. One is the estimation of the vibration velocity through the finite difference approximation of the displacement; another is the phase delay of the electromagnetic actuator and the related amplifier. Also worthy of consideration are the phase lag effects of the A/D and D/A converters while the signal goes through them, and the influence of the low-pass filter if employed. In what follows, these factors will be examined and presented in appropriate analytical models.

3.2.1. *A/D and D/A*

The A/D converter produces time delay for the displacement signals detected by the sensors, while the D/A converter leads to delay for the control signal fed to the actuator. These phase lags are directly related to the sampling time T*, and can be reasonably assumed to take the form of e^{-sT}. To check this, a simple experiment, as depicted in Figure 3, has been conducted to measure the transfer function of a A/D and D/A system. The sampling time used is 0.5 ms (2 kHz) in this case. In Figure 4 is shown the measured transfer function in comparison to that of the term e^{-2sT}. One can see that there is a good agreement between them below about 400 Hz.

3.2.2. *Approximate differential*

In the control system examined here, the velocity signal is not directly measured, but is estimated through approximation of the finite difference of the displacement; that is, the approximate differential. This approximation is also directly related to the sampling time T and will introduce phase lag too. In Figure 5 is shown the experiment arrangement to measure the transfer function of this approximation differentiation element, that can be described, in theory, by $s/(1 + Ts)$. In Figure 6 is given the experiment result compared with the calculated result. With sampling frequency of 2 kHz, these two results also showed good agreement below 400 Hz.

* Also called the sampling rate: its inverse is called the sampling frequency in this paper.

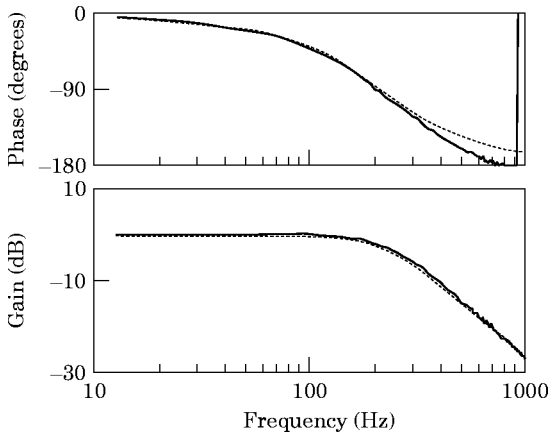

Figure 10. Bode plots of the two-order low-pass filter. ———, Measured; ------, theory.

It is worth noting here that the influence of the sampling rate on the phase lag is profoundly related to the problem of waveform perception. With a sampling time of 0·5 ms (2 kHz), the vibration waveform below 200 Hz can be obtained well, while that above 400 Hz cannot be detected. The highest frequency of the vibration that can be perceived is 1/5 of the sampling frequency. This explains why in the above two cases the experiments differ from the calculations over 400 Hz. As the sampling frequency increases, the frequency range with good agreement will also increase. This has been tested by other experiments using different sampling frequencies.

3.2.3. *Amplifier and actuator*

In this study, the self-made electromagnetic actuator and the corresponding power amplifier are employed for supplying control force. The structure of this actuator is depicted in Figure 7, which can be assumingly represented by an equivalent circuit consisting of coil and resistor, as shown in Figure 8. While the electromagnetic force is in phase with the current passing through the circuit, it is not in phase with the voltage supplied as the control signal. This phase difference can be obtained by introducing a very small resistor in the circuit (R_s in Figure 8) and measuring the voltage fall of it. In Figure 8, the gain of the amplifier is $G = 10$ (20 dB), the resistance of the actuator is measured to

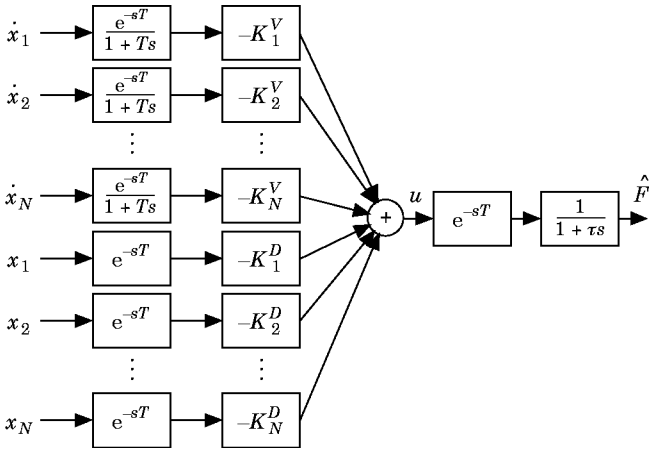

Figure 11. A diagram of the practical control system.

be $R = 5\Omega$ and the appended resistor is $R_s = 0{\cdot}5\Omega$. Thus the transfer function between the input signal u and the monitor signal u_s is expected to be

$$\frac{u_s}{u} \approx G\,\frac{R_s/R}{1 + sL/R} = \frac{1}{1 + \tau s}, \tag{16}$$

τ is called the time constant, $\tau = L/R$.

In Figure 9 is displayed the measured transfer function and the calculated one, with the time constant being 2.5e − 3 s. These two results are in some, though not so good, agreement, which makes it reasonable to present the amplifier and actuator by the one order system with a suitable time constant (this case it is 2.5e − 3 s).

It should be mentioned that this type of electromagnetic actuator not only generates active control force but also exerts passive damping to the structure. The passive damping also exists whether the control is on or off.

3.2.4. *Low-pass filter*

Since the control design is based on a reduced order model, the higher plate modes that are not considered might lead to spillover problems in some cases [13]. A low-pass filter is usually recommended to cut off the high frequency components in the control signal in order to avoid such problems. A two-order analog low-pass filter can be represented by the following transfer function, with suitable parameters for the angular cut-off frequency ω_n and damping factor ζ:

$$lpf(s) = \frac{\omega_n^2}{s^2 + 2\zeta\omega_n s + \omega_n^2}. \tag{17}$$

In Figure 10 is shown the measured transfer function of an analog filter with a cut-off frequency of 220 Hz, in comparison with the calculated one based on equation (17) with $\zeta = 0{\cdot}7$. One can see that they are in very good agreement when below 1 kHz.

3.3. ACTUAL CONTROL FORCE

In the above the transfer functions of the various elements have been discussed. After incorporating these effects into the ideal system shown in Figure 2, an improved one is obtained as illustrated in Figure 11, that can closely represent the practical control system. As a result, the control force becomes

$$\hat{F} = -\frac{e^{-2sT}}{(1 + Ts)(1 + \tau s)}\left(\sum_{n=1}^{N} K_n^V \dot{x}_n + (1 + Ts)\sum_{n=1}^{N} K_n^D x_n\right). \tag{18}$$

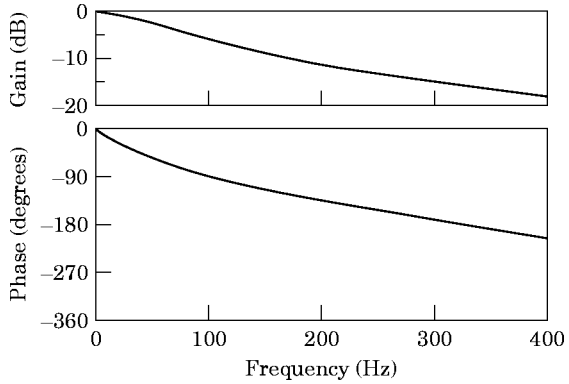

Figure 12. The difference between the actual and the ideal forces: $\tau = 2{\cdot}5$ ms, $T = 0{\cdot}25$ ms, positive polarity.

This is the actual force that is applied to the structure in reality. Comparing with the ideal control force in equation (15) yields the difference between the actual force and the ideal one:

$$\frac{\hat{F}}{F} = \frac{\omega_c^2 e^{-2sT}}{s^2 + 2\xi\omega_c s + \omega_c^2} \frac{\left(\sum_{n=1}^{N} K_n^V \dot{x}_n + (1 + Ts)\sum_{n=1}^{N} K_n^D x_n\right)}{\left(\sum_{n=1}^{N} K_n^V \dot{x}_n + \sum_{n=1}^{N} K_n^D x_n\right)}, \tag{19}$$

where

$$\omega_c = 1/\sqrt{T\tau}, \qquad \xi = (T + \tau)/2\sqrt{T\tau}. \tag{20a, b}$$

What is of most interest is the phase relationship between these two forces. It is reasonable to assume that the phase difference is mainly determined by the first part in the right side of equation (19) (an examination of this is shown in the Appendix). The smaller the phase difference, the better the control results are. Recalling the fundamental principle of active noise control, it should be said that the absolute value of the phase difference should not exceed 90 degrees; otherwise, it would lead to positive feedback and deteriorate robustness.

Let us consider another case in which the polarity of the control signal from D/A board is reversed: then equation (19) becomes

$$\frac{\hat{F}}{F} = -\frac{\omega_c^2 e^{-2sT}}{s^2 + 2\xi\omega_c s + \omega_c^2} \frac{\left(\sum_{n=1}^{N} K_n^V \dot{x}_n + (1 + Ts)\sum_{n=1}^{N} K_n^D x_n\right)}{\left(\sum_{n=1}^{N} K_n^V \dot{x}_n + \sum_{n=1}^{N} K_n^D x_n\right)}. \tag{21}$$

3.4. DISCUSSION

The optimal state feedback gain obtained by the LQ control theory is used to produce a control force that will be contrary in phase to the structure vibration that is to be suppressed. This gain is calculated on the basis of the structure dynamics and the hypothesis that the control system possesses linear ideal frequency characteristics, as

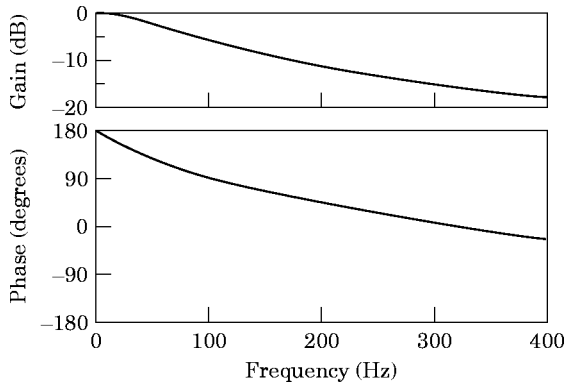

Figure 13. The difference between the actual and the ideal forces: $\tau = 2{\cdot}5$ ms, $T = 0{\cdot}25$ ms, negative polarity.

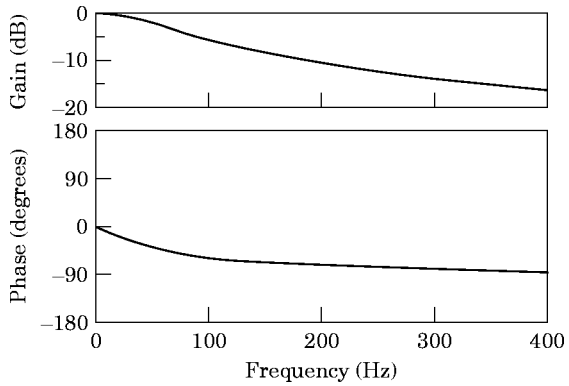

Figure 14. The difference between the actual and the ideal forces: $\tau = 2{\cdot}5$ ms, $T = 0{\cdot}01$ ms, positive polarity.

demonstrated in section 2. However, as one can see from the above examination, the designed control fore is not correctly applied to the structure due to the non-ideal characteristics of the practical control system from the A/D and D/A convertors to the amplifier and actuator, in addition to the systematic limitation inherent in the algorithm used. Careful examination of these factors is very important in order to reach good results with confidence.

With the analytical model developed in the above section, one can conveniently monitor the phase difference between the actual control force and the designed one, as long as the sampling rate of the A/D convertor and the time constant of the actuator are given. This is useful for explaining the control results, predicting the control performance and finding ways to improve it.

In Figure 12 are shown the magnitude and phase of the first part on the right side of equation (19) with sampling time $T = 0{\cdot}25$ ms, time constant $\tau = 2{\cdot}5$ ms, as calculated by Matlab (in all of the following calculations, the second term on the right side of equation (19) is not considered). One can see that at low frequencies (below 100 Hz) the phase lag is less than 90 degrees, while at mid–high frequencies it is larger than 90 degrees. This means that the control can only be realized effectively at rather low frequency. In Figure 13 are shown the results when the polarity of the control force is reversed. It is interesting to notice that at wide mid-high

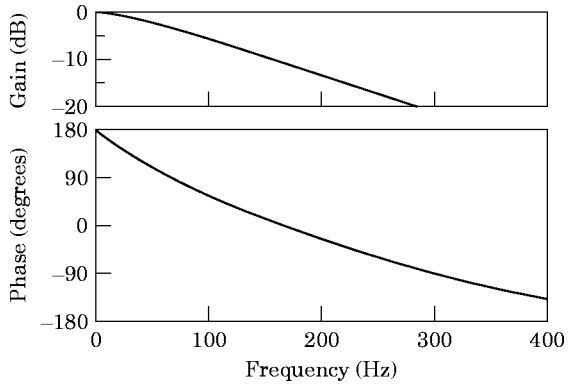

Figure 15. The difference between the actual and the ideal forces with the law-pass filter: $\tau = 2{\cdot}5$ ms, $T = 0{\cdot}25$ ms, LPF cut-off frequency is 220 Hz, negative polarity.

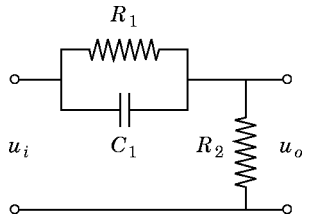

Figure 16. The phase-lead compensation network.

frequency range the phase difference (phase lead and lag) is within the limit of ± 90 degrees, while that below 100 Hz is over this limit. This implies that the higher frequency modes can be correctly controlled but the low frequency modes may be unstable. If the sampling rate is increased to as high as 0·01 ms (100 kHz), then the phase difference between the actual and the ideal forces is within the limit of ± 90 degrees below 400 Hz, as displayed in Figure 14. This means that all the concerned modes below 400 Hz may be controlled at the same time. Increasing the sampling frequency even more, it is found that the result does not improve much, implying that the sampling related factors are now not the main cause for the phase lag, but that the electromagnetic actuator plays the main role.

The influence of the low-pass filter on the phase lag problem can also be easily considered in the framework of the above analysis. If a hardware filter is introduced into the control loop for filtering the control signal, let the filter be represented by a two-order system with an angular cut-off frequency of ω_n and a damping factor of $\zeta = 0{\cdot}7$, as described in equation (17), then the relationship between the actual force and the ideal force is

$$\frac{\hat{F}}{F} \approx \pm \frac{\omega_n^2}{s^2 + 2\zeta\omega_n s + \omega_n^2} \frac{\omega_c^{2e-2sT}}{s^2 + 2\xi\omega_c s + \omega_c^2}, \tag{22}$$

in which "+" refers to positive polarity and "−" to negative polarity of the control signal. With positive polarity, it is clear that the filter will further aggravate the phase lag; while with negative polarity, the phase lag in the filter can somewhat compensate the phase lead which has resulted from the reversal of the control signal polarity, and might result in some good effects in certain frequency range. For example, in the case of 4 kHz sampling frequency, if a filter with cut-off frequency of 220 Hz is introduced into the control system with negative polarity of the control signal, the phase difference between the actual and

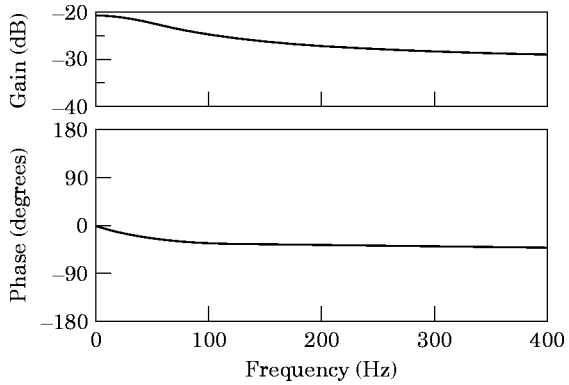

Figure 17. The difference between the actual and the ideal forces with the phase-lead compensation: $\tau = 2{\cdot}5$ ms, $T = 0{\cdot}01$ ms, positive polarity.

the designed forces becomes as shown in Figure 15. It is reasonable to say, in contrast to Figure 13, that the control performance over the frequency range from about 70 Hz to 200 Hz would be improved. As a rule of thumb, the hardware filter should be used with care in implementing a feedback control system. An alternative is to use a software-based digital filter that can be conveniently modeled in an augmented system [14], so that the phase lag of the filter can be taken into account.

Equation (19) and the foregoing calculation demonstrate that, in addition to the lag in phase, the physical system also acts in someway as a low-pass filter in view of the reduction of the gain of the control force. Although this is helpful for eliminating the high frequency components in the control signal which may evoke spillover of unconsidered high modes, it also reduces the energy required for effective control, especially for high controlled modes. Fortunately, the magnitude of the control force can be adjusted easily by changing the feedback gain through adjustment of the weighting factor r in equation (8). In fact, in the present study, the feedback gains with different values are prepared and the best one (strongest but without spillover or saturation) is selected through experiment.

The condition in judging the control performance has to be emphasized: whether the absolute value of the phase difference of the actual and the designed forces exceeds 90 degrees. If so, even for the controllable modes, "spillover" may occur. This kind of "spillover" is due to the deficiency in the control system and is in nature different from that owing to omitted high modes [13]. Even if this phase difference is within the ± 90 degrees limit but is far from zero, as in the case of Figure 14, the control effect would be considerably discounted. From the point of view of control energy, the control would be "expensive" since more power than necessary is required, and perhaps the majority of the power is wasted as "imaginary" power.

4. COMPENSATION OF PHASE LAGS

Now that one can monitor the phase lag of the control system, it becomes natural to obviate it by some means. In previous sections, it has been demonstrated that by using a high speed signal processor, such as the DSP devices that are now popular instruments in the active noise and vibration control community, the phase lags resulting from the sampling speed can be greatly reduced. However, as shown in Figure 14, the phase shift in this case is still fairly large, although within the limit of ± 90 degrees, so that the control performance, particularly over high frequencies, would be somewhat discounted. In this section it is intended to eliminate this actuator-dominated phase lag through some compensation techniques.

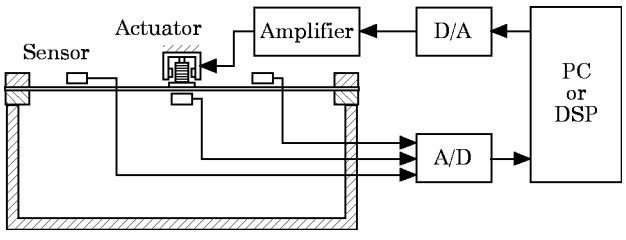

Figure 18. The experimental set-up.

4.1. COMPENSATION NETWORK

A simple method makes use of a phase-lead network [15], as shown in Figure 16. The transfer function of this network is given by

$$G_c(s) = \frac{u_o}{u_i} = \frac{1}{\alpha}\frac{\alpha T_d s + 1}{T_d s + 1}, \tag{23}$$

where,

$$\alpha = \frac{(R_1 + R_2)}{R_2}, \qquad T_d = \frac{R_1 R_2}{R_1 + R_2} C_1 .$$

Incorporating this transfer function into equation (19), one can examine the effects of the phase compensation and adjust the associated parameters. For example, choosing the parameters as $R_1 = 10\ \text{k}\Omega$, $R_2 = 1\ \text{k}\Omega$, and $C_1 = 0{\cdot}1\ \mu\text{F}$, the phase difference between the actual force and the ideal force with this compensation network is calculated as shown in Figure 17. Evidently, this phase-lead compensation circuit is very effective to compensate the phase lag at designed high frequencies, while exerting no influence at low frequencies. One can also see from Figure 17 that the magnitude of the practical control force is greatly reduced by this compensation circuit. This problem can be solved by increasing the gain of the power amplifier of the actuator accordingly.

4.2. MODELLING OF THE ACTUATOR

As has been emphasized, the time delay of the electromagnetic actuator and the related amplifier employed in this research play a leading role in the phase delay of the control

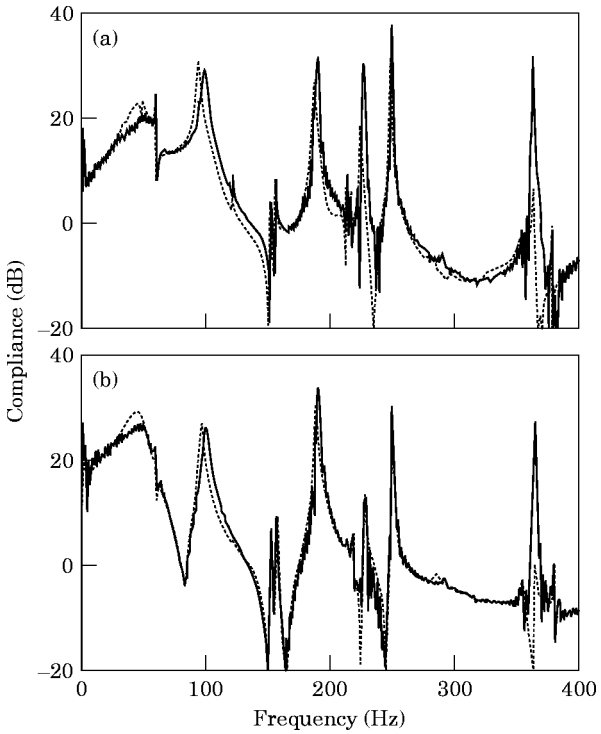

Figure 19. The experimental results under the condition of $T = 0{\cdot}25$ ms and positive polarity. ———, Control on; -----, control off. (a) Exciting near point 2 and picking up at point 1; (b) exciting near point 1 and picking up at point 1.

loop when using the DSP device with high sampling and processing speed. Reference [16] has pointed out the time delay problem of an electromagnetic dynamic absorber that is very similar to the actuator used in this research, and suggested a method for eliminating this problem by feeding back the control current passing through the coil to the controller as an additional state variable. This technique will be adopted in this paper to improve the performance of the electromagnetic actuator.

On this occasion, the assumption of an ideal actuator is relaxed, and the control force in equation (1a) is regarded as being proportional to the current passing through the actuator, rather than to the voltage:

$$f_a = K_I I. \tag{24}$$

Here K_I is the current–force coefficient, which can be approximated by $K_t R$. It has been considered that the electromagnetic actuator can be approximately represented by an equivalent circuit consisting of a coil and a resistor (Figure 8). On the basis of this model, the control signal u and the current I have the following relationship:

$$u = (L\dot{I} + RI)/G, \tag{25}$$

in which G is the gain of the power amplifier of the actuator.

Defining a new state vector $\mathbf{X}$ that is composed of the vibration velocities and displacements at nine mass points *and* the control current

$$\mathbf{X} = [\dot{x}_1 \quad \dot{x}_2 \quad \cdots \quad \dot{x}_9 \quad x_1 \quad x_2 \quad \cdots \quad x_9 \quad I]^{\mathrm{T}}, \tag{26}$$

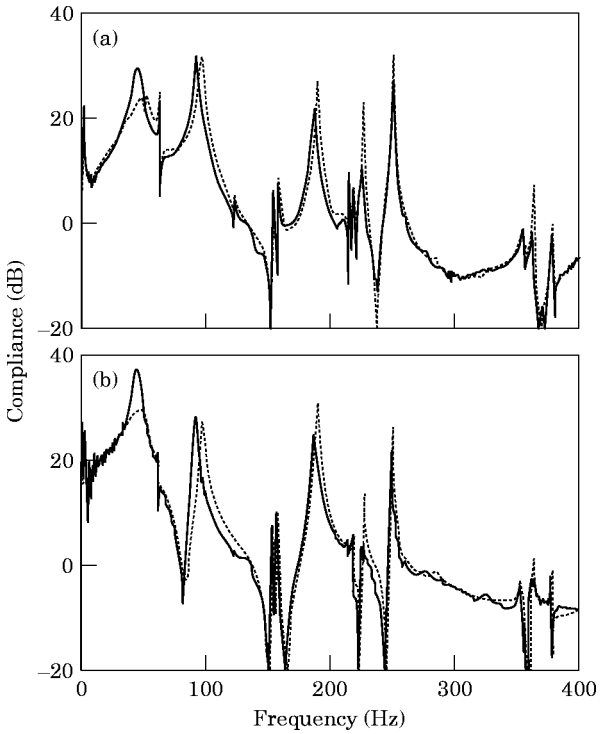

Figure 20. The experimental results under the condition of $T = 0{\cdot}25$ ms and negative polarity. ———, Control on; -----, control off. (a) Exciting near point 2 and picking up at point 1; (b) exciting near point 1 and picking up at point 1.

the new state matrix **A** can be obtained as

$$\mathbf{A} = \begin{bmatrix} -\mathbf{M}^{-1}\mathbf{C} & -\mathbf{M}^{-1}\mathbf{K} & K_I/m_1 \\ & & 0 \\ \mathbf{I} & \mathbf{0} & \vdots \\ & & 0 \\ 0 \quad \cdots & 0 & -1/\tau \end{bmatrix}_{19 \times 19}. \tag{27}$$

Accordingly, the state matrix **b** is redefined as

$$\mathbf{b} = [0 \quad 0 \quad 0 \quad 0 \quad 0 \quad 0 \quad 0 \quad 0 \quad 0 \quad 0 \quad 0 \quad 0 \quad 0 \quad 0 \quad 0 \quad 0 \quad 0 \quad 0 \quad G/R\tau]^{\mathrm{T}}. \tag{28}$$

This is a new system that has accounted for the characteristics of the electromagnetic actuator in the system model. The control design of the new system takes completely the same form as that described by equations (8)–(14) in section 2, except for the transformation matrix:

$$\mathbf{S} = \begin{bmatrix} 1 & 0 & 0 & 0 & 0 & 0 & 0 & 0 & 0 & 0 & 0 & 0 & 0 & 0 & 0 & 0 & 0 & 0 & 0 \\ 0 & 1 & 0 & 0 & 0 & 0 & 0 & 0 & 0 & 0 & 0 & 0 & 0 & 0 & 0 & 0 & 0 & 0 & 0 \\ 0 & 0 & 0 & 0 & 0 & 0 & 0 & 1 & 0 & 0 & 0 & 0 & 0 & 0 & 0 & 0 & 0 & 0 & 0 \\ 0 & 0 & 0 & 0 & 0 & 0 & 0 & 0 & 0 & 1 & 0 & 0 & 0 & 0 & 0 & 0 & 0 & 0 & 0 \\ 0 & 0 & 0 & 0 & 0 & 0 & 0 & 0 & 0 & 0 & 1 & 0 & 0 & 0 & 0 & 0 & 0 & 0 & 0 \\ 0 & 0 & 0 & 0 & 0 & 0 & 0 & 0 & 0 & 0 & 0 & 0 & 0 & 0 & 0 & 0 & 1 & 0 & 0 \\ 0 & 0 & 0 & 0 & 0 & 0 & 0 & 0 & 0 & 0 & 0 & 0 & 0 & 0 & 0 & 0 & 0 & 0 & 1 \end{bmatrix}. \tag{29}$$

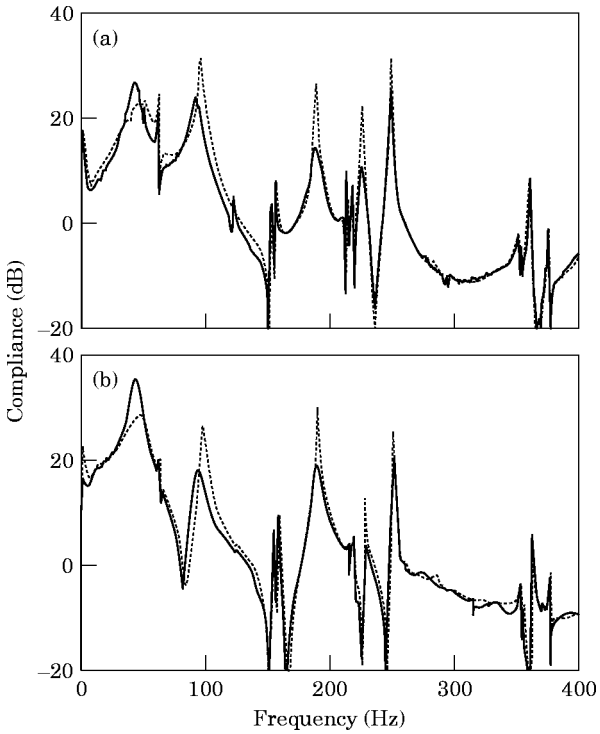

Figure 21. The experimental results under the condition of $T = 0{\cdot}25$ ms and negative polarity with the low pass filter (the cut-off frequency is 220 Hz). ———, Control on; -----, control off. (a) Exciting near point 2 and picking up at point 1; (b) exciting near point 1 and picking up at point 1.

It is worth pointing out that in the newly obtained gain vector, the last element is the feedback gain for the new state variable—the control current.

5. EXPERIMENTS

Experiments with the aim of controlling the modal vibration and the noise radiation of the plate have been carried out to test the above analysis. As described in section 2, three non-contact displacement sensors (gap sensor) and one electromagnetic actuator are employed according to the sub-optimal control theory. The actuator is fixed at the plate centre and the sensors are located at mass points 1, 2 and 8 respectively (please refer to Figure 1). The experimental set-up is sketched in Figure 18. With this arrangement, four-vibration modes of the plate are expected to be controlled as explained in section 2: they are the first (44 Hz), the third (98 Hz), the eighth (189 Hz) and the twelfth modes (253 Hz). The vibration control effects are evaluated by measuring the transfer function (compliance) of the plate under impulse excitation by hammer. For brevity, only the results for two sets of conditions are given; that is, exciting near point 2 while picking up at point 1, and exciting near point 1 while picking up at point 1.

5.1. CONTROL WITHOUT COMPENSATION

5.1.1 *The PC as a controller*

For the purpose of verifying the analysis in section 3, a few results using a microcomputer (NEC PC98) as the controller are given. The sampling frequency used is

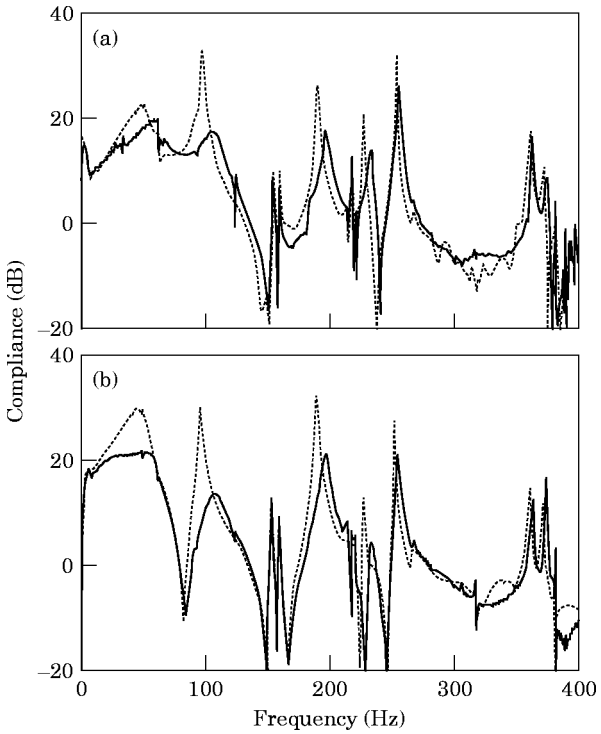

Figure 22. The experimental results under the condition of $T = 0{\cdot}01$ ms and positive polarity. ———, Control on; -----, control off. (a) Exciting near point 2 and picking up at point 1; (b) exciting near point 1 and picking up at point 1.

4 kHz (in this case the maximum sampling frequency that can be properly used is about 5 kHz). In Figure 19 is shown the result in normal condition; that is, the polarity of the control signal is positive. In agreement with the phase condition shown in Figure 12, only the first mode is controlled and the modes above 100 Hz become unstable. In Figure 20 is shown the result with the polarity being reversed. This is not surprising if one considers the phase condition shown in Figure 13, that the first mode becomes unstable but the higher order modes (above 100 Hz) are well controlled. It is interesting to note that some modes that are not considered in the reduced order model (such as the eleventh mode, 228 Hz) are also suppressed. This is probably due to the fact that the actuator is collocated with one sensor. In both Figures 19 and 20, the third mode (98 Hz) is not controlled. In order to improve it, a low-pass filter with a cut-off frequency of about 220 Hz is used for the control signal with the negative polarity, to create the phase relationship as shown in Figure 15. In Figure 21 is given the control result, showing an evident improvement around 100 Hz. In this case the phase shift exceeds the $\pm$ 90 degrees limit above 300 Hz but the system remains stable, since the magnitude of the control signal is greatly reduced. One can see that the function of the low-pass filter has changed in this case; it behaves more like a compensator than a filter.

It should be pointed out that the first mode of the plate does not display a sharp peak in the transfer function diagrams. This is mainly due to the damping effect of the air cavity. In observing these figures, attention should also be paid to the fact that the second mode (about 63 Hz) and several other modes are not controlled; therefore, these modes remain unsuppressed.

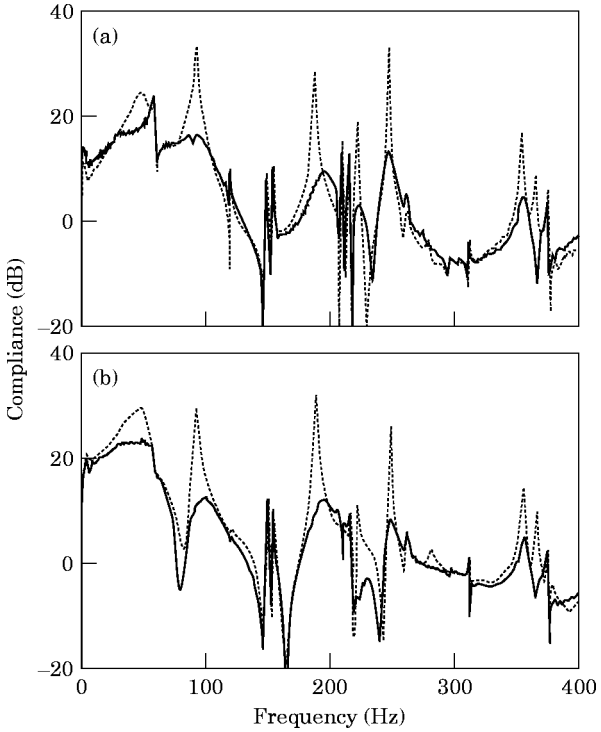

Figure 23. The experimental results under the condition of $T = 0{\cdot}01$ ms and positive polarity with the phase-lead compensation. ———, Control on; -----, control off. (a) Exciting near point 2 and picking up at point 1; (b) exciting near point 1 and picking up at point 1.

The above results confirm the model and analysis presented in this paper about the influence of the phase lags in the control system. They also demonstrate the difficulties of active vibration control in the audio frequency range using a microcomputer based control system that has a relatively low sampling and processing speed.

5.1.2. *The DSP as a controller*

A DSP device (TMS320C40) has also been employed in this experimental study as the controller. With the capacity of high speed processing and the accompanying A/D and D/A boards, the sampling frequency can become as high as 100 kHz. In this case, the phase relationship between the actual control force and the designed one is displayed in Figure 14. As demonstrated by the results shown in Figure 22, the four controlled modes (and also the 11th mode) are simultaneously well suppressed.

It should be mentioned that the above two sets of experiments were conducted at different times, and therefore, the measured transfer functions of the plate without control have altered slightly. One may have noticed that in these results, the controlled peaks have shifted slightly along the frequency axis. This is because the effective stiffness and mass of the closed loop system change a little under the influence of the time delay in the feedback loop, as examined by Fuller *et al*. [2].

In the present investigation, the actuator is collocated with one sensor at the plate centre; the spillover problem due to the unmodelled high modes would therefore be alleviated. It is observed in the experiments that as long as the actual control force is in phase with the designed force (within the ± 90 degrees limit), the closed loop system will be stable; but if the time delay in control system is so large that the actual force is out of phase with

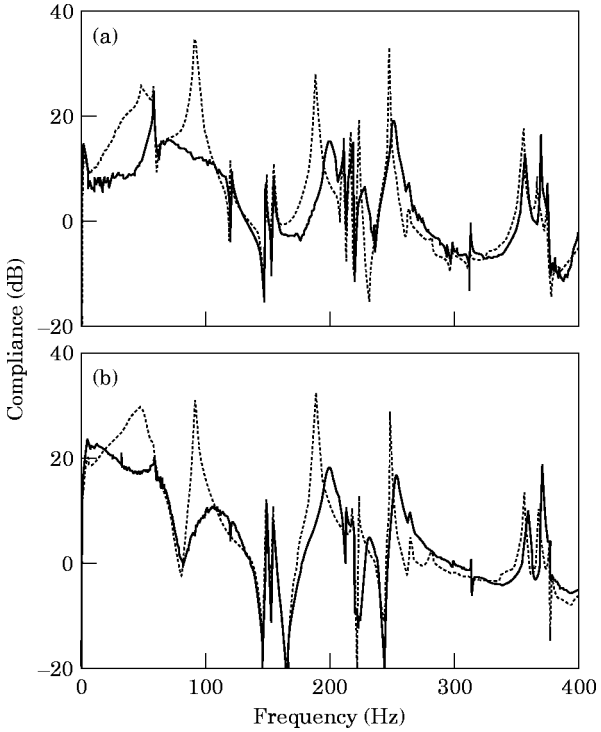

Figure 24. The experimental results under the condition of $T = 0{\cdot}01$ ms and positive polarity with the current feedback. ———, Control on; -----, control off. (a) Exciting near point 2 and picking up at point 1; (b) exciting near point 1 and picking up at point 1.

the designed one (beyond the ± 90 degrees limit), terrible "spillover" will occur. If it was taken for granted that such "spillover" was due to the omitted high modes in the modelling, the conclusion would be misleading.

5.2. CONTROL WITH COMPENSATION

Phase compensation is carried out in the case of the DSP controller, in order further to improve the control performance and probably save control energy, which is mainly hindered by the characteristics of the electromagnetic actuator.

5.2.1. *With compensation network*

In Figure 23 is shown the experimental result with the phase-lead compensation network (Figure 16) being used. This network is placed before the power amplifier, and the gain

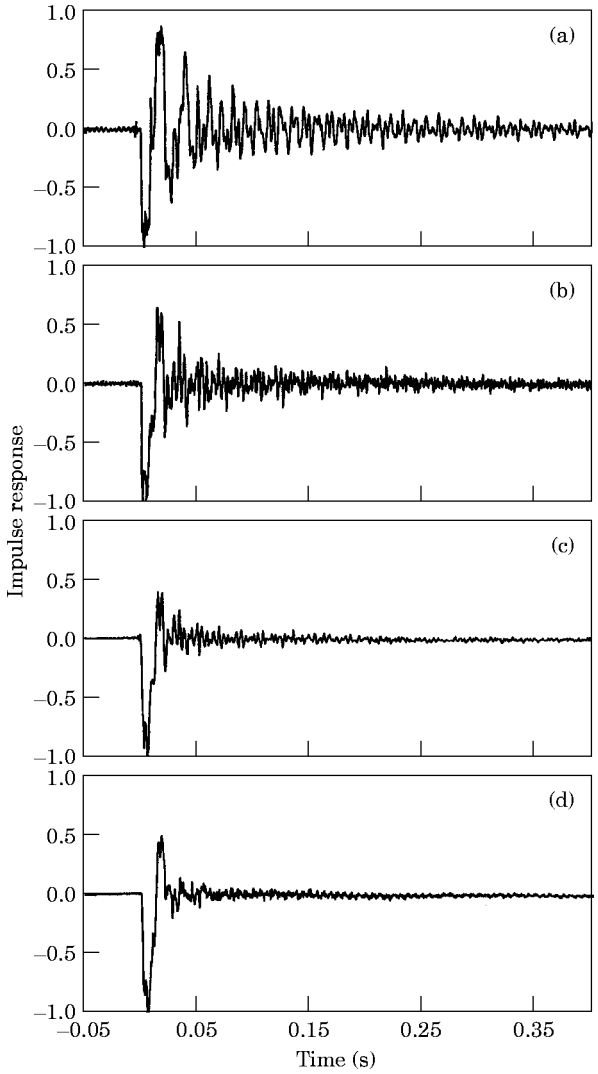

Figure 25. The impulse responses of the plate measured at the plate centre. (a) Control off; (b) control without either the phase-lead compensation or the current feedback, $T = 0{\cdot}01$ ms, positive polarity; (c) control with the current feedback, $T = 0{\cdot}01$ ms, positive polarity; (d) control with the phase-lead compensation, $T = 0{\cdot}01$ ms, positive polarity.

of the amplifier is increased by a factor of ten in order to offset the reduction of the control force magnitude due to the effect of the compensation network. One can see from this figure that all the concerned modes are quite well controlled in reference to the phase condition shown in Figure 17. This result proves the effectiveness of the phase-lead compensation method. It can also serve as a testimony to the analysis presented in section 3.

5.2.2. *With current feedback*

The phase lag elimination method proposed in section 4.2 needs to monitor the control current passing through the actuator. In practice, the measurement of the control current can be realized by measuring the voltage fall over a small resistor introduced into the control circuit (Figure 8). In Figure 24 is shown the experimental result with the control current of the actuator being fed back to the controller. In comparison with the result in Figure 22, the control performance over all the concerned modes has evidently improved with this current feedback method. The improvements can also be clearly observed from the corresponding impulse responses obtained at the plate centre, as shown in Figure 25. In the figure the control results without and with the current feedback are compared to that without control. Also in this figure, the result of the phase-lead compensation is shown for comparison.

The above results show that the method employing the phase-lead compensation network seems to be the appropriate way to reach the best result. The method incorporating the characteristics of the actuator into the system model by current feedback is more fundamental. In essence, it should not be called a "compensation" method. In principle, the optimal feedback gains calculated by modelling the actuator in the control design will account for the time delay of the actuator, and a correct phase for the control force is supposed to be systematically guaranteed. The results given in Figures 24 and 25 show evident improvement in contrast to the results without considering the actuator dynamics (Figure 22), proving that the considerations and the methods are correct. Nevertheless, the control performance at high frequencies seems not to be as good as that by the phase-lead compensation method. The main reason is perhaps that the optimal feedback gains of the whole system involving the actuator dynamics are determined on the observation of the full states of the structure, but in experiments some of the states are dropped in order to use the sub-optimal control theory (only the states at three mass points are observed for the nine mass points model). As a result, the guarantee for the correct phase of the control force under the influence of the actuator time delay might be discounted to some extent.

6. CONCLUSIONS

In this paper the phase lag problem in the feedback control of a clamped flexible plate at audio frequencies with the electromagnetic actuator has been investigated. The analysis and model discussed in this paper allow one to estimte quantitatively the phase shift of the actual control force from that of the designed control force under the influence of the A/D and D/A convertors, the amplifier and actuator, the filter and the approximation differential. It has been found that the control performance is greatly worsened and "spillover" may occur when the phase shift between the actual force and the designed force is over ± 90 degrees. If high speed sampling and processing devices are used, the time delay of the electromagnetic actuator will be the main obstacle for the application of this type of actuator in controlling high frequency vibration and noise. This problem can be

fundamentally solved by accounting for the actuator characteristics in system modelling. The method, which is based on an equivalent circuit consisting of a coil and a resistor, is to monitor the control current passing through the actuator as a state variable and feed it back into the controller. Another method that is simpler and more practical in this case is to employ a phase-lead compensation circuit between the D/A convertor and the power amplifier. The suitable parameters for the circuit can be determined on the basis of the phase lag prediction presented in this paper. As verified by the experiments in this paper, the vibration control performance of the clamped flexible plate has been significantly improved by the proposed methods. The potential of using the electromagnetic actuator to control the structure vibration at the audio frequencies has therefore been demonstrated.

REFERENCES

1. K. Seto 1992 *Proceedings of the* 1*st International Conference on Motion and Vibration Control*, *Yokohama*, *Japan*, 152–158. Trends on active vibration control in Japan.
2. C. R. Fuller, S. J. Elliott and P. A. Nelson 1996 *Active Control of Vibration*. London: Academic Press. See chapters 3 and 6.
3. P. A. Nelson and S. J. Elliott 1992 *Active Control of Sound*. London: Academic Press.
4. V. L. Metcalf, C. R. Fuller, R. J. Silcox and D. E. Brown 1992 *Journal of Sound and Vibration* **153**, 387–402. Active control of sound transmission/radiation from elastic plates by vibration inputs, II: experiments.
5. K. Seto and K. Sawadari 1990 *The Japan Society of Mechanical Engineering International Journal* **33**(3), 453–459. Vibration control of a plate structure by an active control device for reducing noise.
6. W. T. Baumann, F. S. Ho and H. H. Robertshaw 1992 *Journal of the Acoustical Society of America* **92**, 1998–2005. Active structural acoustic control of broadband disturbances.
7. D. R. Thomas and P. A. Nelson 1994 *Proceedings of the* 2*nd International Conference on Motion and Vibration Control*, *Yokohama*, *Japan*, 389–394. Feedback control of sound radiation from a plate excited by a turbulent boundary layer.
8. Z. Wu, V. K. Varadan, V. V. Varadan and K. Y. Lee 1995 *Journal of the Acoustical Society of America* **97**, 1078–1087. Active absorption of acoustic waves using state-space model and optimal control theory.
9. S. J. Dyke, B. F. Spencer, P. Quast and M. K. Sain 1995 *Journal of Engineering Mechanics* **121**(2), 322–338 Role of control–structure interaction in protective system design.
10. K. Seto and S. Mitsuta 1992 *Proceedings of the* 1*st International Conference on Motion and Vibration Control*, *Yokohama*, *Japan*, 152–158. A new method for making a reduced-order model of flexible structures using unobservability and uncontrollability and its application in vibration control.
11. M. Z. Ren, K. Seto and F. Doi 1997 CD-ROM *Proceedings of 1997 ASME Design Engineering Technical Conferences (DETC'97)*, *Sacramento*, *U.S.A.*, paper number: DETC97/VIB-3811. Modeling and feedback control of flexible plate with focus on the modes highly coupled to radiation field.
12. R. L. Kosut 1970 *IEEE Transactions on Automatic Control* **AC-15**(5), 557–563. Suboptimal control of linear time-invariant system subject to control structure constraints.
13. M. J. Balas 1978 *IEEE Transactions on Automatic Control* **AC-23** 673–679. Feedback control of flexible structures.
14. K. Seto, F. Doi, H. Inoue and M. Hisatani 1996 *Proceedings of the* 3*rd International Conference on Motion and Vibration Control*, *Chiba*, *Japan* **2**, 24–29. Structural vibration control for bridge towers under construction (2nd report: a simple robust control and its effectiveness).
15. N. Tominari, K. Seto and Y. Okada 1979 *Analysis and Design of Servo Control Systems*. Tokyo: Corona Publishing. See chapter 5.
16. K. Seto and Y. Furuishi 1991 *Proceedings of ASME Modal Analysis*, *Modeling*, *Diagnostics and Control—Analytical and Experimental*, **DE-Vol. 38**, 263–270. A study on active dynamic absorber.

APPENDIX

Rewrite the second part of the right side of equation (19) as

$$H(s) = \frac{\left(\sum_{n=1}^{N} K_n^V \dot{x}_n + (1 + Ts)\sum_{n=1}^{N} K_n^D x_n\right)}{\left(\sum_{n=1}^{N} K_n^V \dot{x}_n + \sum_{n=1}^{N} K_n^D x_n\right)} = \frac{Nom(s)}{Den(s)}. \tag{A1}$$

It is not feasible to compute the precise phase of this term, since it depends on the state variables of the structure. However, one can evaluate this quantity to some degree. Notice the following relation stands

$$\dot{x}_n = sx_n,$$

one can obtain the phases of $Nom(s)$ and $Den(s)$ respectively as follows:

$$\langle Nom = \arctan \frac{\omega\left(\sum_{n=1}^{N} K_n^V x_n + T\sum_{n=1}^{N} K_n^D x_n\right)}{\sum_{n=1}^{N} K_n^D x_n}, \tag{A2}$$

$$\langle Den = \arctan \frac{\omega\sum_{n=1}^{N} K_n^V x_n}{\sum_{n=1}^{N} K_n^D x_n}. \tag{A3}$$

The values of the gain for the velocity states, K_n^V, and that for the displacement states, K_n^D, are determined by solving the Riccati equation of the system, although there seems to be no distinct relationship between them. However, in the experimental work involved in this paper, it was observed that K_n^D, is usually larger than K_n^V, in absolute value. Nevertheless, the sampling time T is very small, generally four or five orders smaller than unity that is at least one order higher than the order of the difference between K_n^V, and K_n^D. Therefore, there will be no considerable difference between equations (A2) and (A3): that is, the phase of $H(s)$ is very small.